

MULTIPHYSICS MODELING OF THE SPARK PLASMA SINTERING -SPS- PROCESS	العنوان:
Luqman, Muhammad	المؤلف الرئيسي:
Nouari, Saheb(super.)	مؤلفين آخرين:
2014	التاريخ الميلادي:
الظهران	موقع:
1 - 134	الصفحات:
651624	رقم MD:
رسائل جامعية	نوع المحتوى:
English	اللغة:
رسالة ماجستير	الدرجة العلمية:
جامعة الملك فهد للبترول والمعادن	الجامعة:
عمادة الدراسات العليا	الكلية:
السعودية	الدولة:
Dissertations	قواعد المعلومات:
النمذجة، الهندسة الميكانيكية	مواضيع:
<a href="https://search.mandumah.com/Record/651624">https://search.mandumah.com/Record/651624</a>	رابط:

## ABSTRACT

Full Name : Muhammad Luqman  
Thesis Title : Multi-Physics Modeling Of The Spark Plasma Sintering (SPS) Process  
Major Field : Mechanical Engineering  
Date of Degree : March, 2014

Spark plasma sintering (SPS) is defined as a processing technique, which sinters materials using electric current in conjunction with uniaxial pressure. It offers several advantages over conventional techniques like achievement of near-theoretical density and nanocrystalline morphology in extremely shorter sintering durations, avoidance of abnormal grain growth, and clean sample surfaces due to interaction with gaseous plasma. However, the major drawbacks of SPS which are not observed in conventional sintering techniques include difficulty in sintering complex-shaped or large-sized samples, relatively large degree of inhomogeneity in mechanical properties, and charge accumulation especially in insulating powders. Hence in order to achieve the best processing results, it is obligatory to grasp a firm understanding of the kinetics of SPS process. Since experimental methods do not facilitate the in-situ measurement of sintering temperature, pressure, and relative density, one has to rely on computational techniques in order to get a better understanding of the process kinetics. These computational techniques are utilized in predicting the structure-property relationship of the material being sintered, and optimization of the process parameters in order to achieve the best mechanical properties without presence of inhomogeneity. The main

objective of the computational work done in this study is to develop a coupled electrical–thermal–mechanical Finite Element Model of the SPS process. This model has been used to study two different classes of materials – aluminum (an electrical conductor), and alumina (an electrical insulator), where a range of aspect ratios has been considered for each disk-shaped sample. In order to validate the results obtained via computational analysis, a small-scale experimental study is also conducted to determine the relationship between SPS process-parameters and the mechanical properties of sintered sample. Comparison of the results obtained from the computational model with those achieved from the experimental study, indicate that almost all the process parameters as well as mechanical properties are characterized by inhomogeneity within the sintered samples.

## ملخص الرسالة

الاسم الكامل : محمد لقمان

عنوان الرسالة : متعدد الفيزياء نمذجة البلازما التكلس سبارك (SPS). عملية

التخصص : الهندسة الميكانيكية

تاريخ الدرجة العلمية : مارس 2014

يتم تعريف تكلس شرارة البلازما (SPS) كأسلوب معالجة، والتي تكلس المواد باستخدام التيار الكهربائي بالتزامن مع الضغط أحادي المحور. أنها توفر العديد من المزايا أكثر من التقنيات التقليدية مثل تحقيق الكثافة شبه النظرية، وتشكل البلورات النانوية في فترات تكلس قصيرة للغاية، متجنبة نمو الحبوب الغير طبيعية، وسطوح العينات النظيفة بسبب التفاعل مع غازات البلازما. ومع ذلك، فإن العوائق الرئيسية لتكلس شرارة البلازما التي لم تلاحظ في تقنيات التكلس التقليدية تشمل صعوبة في تكلس العينات ذو الأشكال المعقدة أو كبيرة الحجم، نسبيا درجة عالية من عدم التجانس في الخصائص الميكانيكية، وتراكم الشحنات خاصة في عزل المساحيق. وبالتالي من أجل تحقيق أفضل النتائج المعالجة، يجب الامساك بالفهم الراسخ لحركية تكلس شرارة البلازما. و بما أن الطرق التجريبية لا تسهل قياس درجة الحرارة و الضغط و الكثافة النسبية للتكلس أثناء اجراء التجربة، على المرء الاعتماد على التقنيات الحاسوبية من أجل الحصول على فهم أفضل للعملية الحركية. وتستخدم هذه التقنيات الحاسوبية في التنبؤ بعلاقة مميزات البنية للمواد الجاري تكلسها ، والاستفادة المثلى من معايير العملية من أجل تحقيق أفضل الخواص الميكانيكية في غياب عدم التجانس. الهدف الرئيسي من هذا العمل الحسابي في هذه الدراسة هو تطوير عناصر محدودة مقترنة كهربائيا وحراريا وميكانيكيا باستخدام عملية تكلس شرارة البلازما. وقد استخدم هذا النموذج لدراسة فئتين مختلفتين من المواد - الألومنيوم (موصل كهربائي) والألومينا (عازل كهربائي). حيث تم اعتبار مجموعة ذو نسب مختلفة من نسب العرض للطول لكل عينة على شكل القرص. من أجل التحقق من صحة النتائج التي تم الحصول عليها عن طريق التحليل الحسابي، أجرت دراسة تجريبية على نطاق ضيق لتحديد العلاقة بين عملية المتغيرات لتكلس شرارة البلازما والخواص الميكانيكية للعينة المتكلسة.

المقارنة بين النتائج تم الحصول عليها من النموذج الحسابي مع تلك التي تحققت من دراسة تجريبية، تشير إلى أن جميع المتغيرات وكذلك الخواص الميكانيكية تتميز بعدم التجانس في حدود العينات المتكلسة.

MULTIPHYSICS MODELING OF THE SPARK PLASMA SINTERING -SPS- PROCESS	العنوان:
Luqman, Muhammad	المؤلف الرئيسي:
Nouari, Saheb(super.)	مؤلفين آخرين:
2014	التاريخ الميلادي:
الظهران	موقع:
1 - 134	الصفحات:
651624	رقم MD:
رسائل جامعية	نوع المحتوى:
English	اللغة:
رسالة ماجستير	الدرجة العلمية:
جامعة الملك فهد للبترول والمعادن	الجامعة:
عمادة الدراسات العليا	الكلية:
السعودية	الدولة:
Dissertations	قواعد المعلومات:
النمذجة، الهندسة الميكانيكية	مواضيع:
<a href="https://search.mandumah.com/Record/651624">https://search.mandumah.com/Record/651624</a>	رابط:

# TABLE OF CONTENTS

ACKNOWLEDGMENTS .....	iv
TABLE OF CONTENTS.....	v
LIST OF FIGURES .....	viii
LIST OF TABLES .....	xiv
NOMENCLATURE .....	xv
ABSTRACT.....	xvi
ملخص الرسالة.....	xviii
CHAPTER 1 .....	1
INTRODUCTION .....	1
1.1    SPARK PLASMA SINTERING (SPS) .....	2
1.1.1    Instrumentation.....	2
1.1.2    Sintering procedure.....	2
1.1.3    Electrical transport in SPS process .....	3
1.1.4    Heating mechanism in SPS process.....	4
1.1.5    Loading mechanism in SPS process .....	6
1.1.6    Advantages of SPS .....	6
1.1.7    Difficulties in SPS process .....	8
1.1.8    Differences between conventional and non-conventional sintering mechanisms .....	8
1.2    MOTIVATION .....	9
1.3    OBJECTIVES .....	10
CHAPTER 2 .....	11
LITERATURE REVIEW .....	11
2.1    THERMAL-ELECTRICAL MODELING .....	12

2.2	STRUCTURAL MODELING .....	22
CHAPTER 3 .....		27
EXPERIMENTAL STUDY.....		27
3.1	INTRODUCTION.....	27
3.2	EXPERIMENTAL TECHNIQUES .....	27
3.2.1	Particles' Size Analysis .....	27
3.2.2	X-Ray Diffraction.....	28
3.2.3	Micro-hardness Testing .....	30
3.2.4	Scanning Electron Microscope .....	31
3.3	RAW MATERIALS.....	32
3.3.1	Aluminum powder.....	32
3.3.2	Alumina powder .....	34
3.4	SPARK PLASMA SINTERING (SPS) .....	36
3.5	RESULTS.....	38
3.5.1	Sample Preparation.....	38
3.5.2	Hardness Test .....	38
3.5.3	Microstructure .....	41
CHAPTER 4 .....		44
ELECTRICAL-THERMAL MODEL .....		44
4.1	INTRODUCTION.....	44
4.2	THE MODEL.....	45
4.2.1	Mathematical Model.....	45
4.2.2	Model in COMSOL Multiphysics .....	49
4.3	RESULTS & DISCUSSION.....	55
4.3.1	General Observations about the whole system .....	55

4.3.2	Validation of the developed model.....	61
4.3.3	CASE-I .....	63
4.3.4	CASE-II.....	75
CHAPTER 5	.....	82
STRUCTURAL MODEL	.....	82
5.1	INTRODUCTION.....	82
5.2	THE MODEL.....	82
5.2.1	Mathematical model .....	82
5.2.2	Model in COMSOL Multiphysics .....	85
5.3	RESULTS AND DISCUSSIONS .....	86
5.3.1	Validation of the developed model.....	86
5.3.2	CASE-I .....	89
5.3.3	CASE-II.....	113
CHAPTER 6	.....	135
CONCLUSIONS & RECOMMENDATIONS	.....	135
6.1	CONCLUSIONS.....	136
6.2	RECOMMENDATIONS .....	137
REFERENCES	.....	139
VITAE	.....	143



## LIST OF FIGURES

Figure 1: Schematic of SPS Process [1] .....	2
Figure 2: Different pulse patterns in pulsed DC power supply [2].....	4
Figure 3: SPS Sintering mechanism; Plasma heating (left), & Joule heating (right) [3]....	5
Figure 4: Densification mechanism in SPS [3].....	6
Figure 5: Comparison of sintering time and temp. Of SPS and conventional sintering [6].....	7
Figure 6: Integration domain and boundary conditions of the model proposed by Raichenko and Chernikova [9]. .....	12
Figure 7: Integration domain and boundary conditions of the model proposed by Yoneya and Ikeshoji [10].....	14
Figure 8: Integration domain of the model proposed by Matsugi et al [13].....	16
Figure 9: Simulation results for die diameter and die height at a sample center temperature of 1,800°C. Solid points represent simulations including radiation, and hollow points are simulation results with die wall radiation blocked. [5] .....	19
Figure 10: Complex shaped part sintered by Spark Plasma Sintering [21] .....	21
Figure 11: Schematic of X-Rays diffraction.....	29
Figure 12: Schematic of micro-hardness test.....	31
Figure 13: Electron-sample interactions. ....	32
Figure 14: Particle size distribution of as-received aluminum powder. ....	33
Figure 15: Microstructure of as-received aluminum powder. ....	33
Figure 16: XRD spectrum of as received Aluminum powder .....	34
Figure 17 : Particle size distribution of as-received alumina powder.....	35
Figure 18: Microstructure of as-received alumina powder.....	35
Figure 19: XRD spectrum of as received Alumina powder.....	36
Figure 20: Die-punch system during sintering of alumina samples .....	37
Figure 21: Positions of the hardness test.....	39

Figure 22: Hardness (HV) along the radius at different heights in aluminum sample .....	40
Figure 23: Hardness (HV) along the height at different radial positions in aluminum sample .....	40
Figure 24: Hardness (HV) along the radius at different heights in alumina sample.....	41
Figure 25: Hardness (HV) along the height at different radial positions in alumina sample .....	41
Figure 26: SEM micrographs of the aluminum sample at 1000x magnification at different locations: A1, A3, A5, C1, C3, C5, E1, E3, & E5 .....	42
Figure 27: SEM micrographs of the aluminum sample at 500x magnification at different locations: A1, A3, A5, C1, C3, C5, E1, E3, & E5 .....	43
Figure 28: Schematic of the die-punch-specimen system in SPS process.....	49
Figure 29: Model Geometry in COMSOL Multiphysics environment.....	50
Figure 30: Domains and boundaries in the model. ....	51
Figure 31: The Applied voltage .....	52
Figure 32: Meshes used in the model: Left) mapped, & Right) triangular.....	53
Figure 33: Surface Current density contour plot for sample height=50 mm, at 650s.....	56
Figure 34: Surface Current density contour plot for sample height=100 mm, at 650s.....	56
Figure 35: Surface Temperature contour plot for sample height=50mm, at t=650s.....	57
Figure 36: Surface Temperature contour plot for sample height=100mm, at t=650s.....	58
Figure 37: Graph showing the temperature evolution in punches .....	58
Figure 38: Graph showing the temperature evolution in the sample .....	59
Figure 39: Graph showing average temperature evolution in sample for different sample heights.....	59
Figure 40: Divisions in the sample. ....	60
Figure 41: Current density distribution along the radius: Left) this study, & Right) F. Mechighel et. Al. [32].....	61
Figure 42: Temperature distribution along the radius: Left) this study, & Right) F. Mechighel et. Al [32].....	62

Figure 43: Current density plots at: (left) $t=350s$ , & (right) $t=600s$ .....	65
Figure 44: (Left) Current density in the system, & (right) corresponding Total heat source in the system at $t=1200s$ .....	65
Figure 45: Current density distribution along radius at different axial positions for different sample thicknesses: row1) height=10mm, row 2) height=50mm, & row 3) height=100mm .....	66
Figure 46: Current density distribution along height at different radial positions for different sample thicknesses: row1) height=10mm, row 2) height=50mm, & row 3) height=100mm .....	67
Figure 47: Current density evolution at different locations for different sample thicknesses: row1) height=10mm, row 2) height=50mm, & row 3) height=100mm .....	68
Figure 48: Temperature distribution in the system at different timings at: (left) $t=600s$ , & (right) $t=1200s$ . .....	70
Figure 49: Temperature distribution along radius at different axial positions for different sample thicknesses: row1) height=10mm, row 2) height=50mm, & row 3) height=100mm .....	71
Figure 50: Temperature distribution along height at different radial positions for different sample thicknesses: row1) height=10mm, row 2) height=50mm, & row 3) height=100mm .....	72
Figure 51: Temperature evolution at different locations for different sample thicknesses: row1) height=10mm, row 2) height=50mm, & row 3) height=100mm .....	73
Figure 52: Current density evolution at different locations for different sample thicknesses: row1) height=10mm, row 2) height=50mm, & row 3) height=100mm .....	77
Figure 53: Temperature distribution along radius at different axial positions for different sample thicknesses: row1) height=10mm, row 2) height=50mm, & row 3) height=100mm .....	78
Figure 54: Temperature distribution along height at different radial positions for different sample thicknesses: row1) height=10mm, row 2) height=50mm, & row 3) height=100mm .....	79
Figure 55: Temperature evolution at different locations for different sample thicknesses: row1) height=10mm, row 2) height=50mm, & row 3) height=100mm .....	80

Figure 56: The Applied pressure.....	86
Figure 57: Axial stress distribution along the radius in the sample: Left) this study, & Right) F. Mechighel et. Al [32] .....	87
Figure 58: Radial stress distribution along the radius in the sample: Left) this study, & Right) F. Mechighel et. Al [32] .....	88
Figure 59: Current density along height at different radial positions for different sample thicknesses: row1) height=10mm, row 2) height=50mm, & row 3) height=100mm .....	90
Figure 60: Current density along radius at different axial positions for different sample thicknesses: row1) height=10mm, row 2) height=50mm, & row 3) height=100mm .....	91
Figure 61: Current density evolution at different axial positions for different sample thicknesses: row1) height=10mm, row 2) height=50mm, & row 3) height=100mm .....	92
Figure 62: Height-wise temperature distribution at different radial positions for different sample thicknesses: row1) height=10mm, row 2) height=50mm, & row 3) height=100mm .....	94
Figure 63: Radius-wise temperature distribution at different radial positions for different sample thicknesses: row1) height=10mm, row 2) height=50mm, & row 3) height=100mm .....	95
Figure 64: Temperature evolution at different axial positions for different sample thicknesses: row1) height=10mm, row 2) height=50mm, & row 3) height=100mm .....	96
Figure 65: Height-wise von-Mises stress distribution at different radial positions for different sample thicknesses: row1) height=10mm, row 2) height=50mm, & row 3) height=100mm .....	98
Figure 66: Radius-wise von-Mises stress distribution at different axial positions for different sample thicknesses: row1) height=10mm, row 2) height=50mm, & row 3) height=100mm .....	99
Figure 67: Von-Mises stress evolution at different axial positions for different sample thicknesses: row1) height=10mm, row 2) height=50mm, & row 3) height=100mm .....	100
Figure 68: Height-wise axial stress distribution at different radial positions for different sample thicknesses: row1) height=10mm, row 2) height=50mm, & row 3) height=100mm .....	102

Figure 69: Radius-wise axial stress distribution at different axial positions for different sample thicknesses: row1) height=10mm, row 2) height=50mm, & row 3) height=100mm .....	103
Figure 70: Axial stress evolution at different axial positions for different sample thicknesses: row1) height=10mm, row 2) height=50mm, & row 3) height=100mm .....	104
Figure 71: Height-wise radial stress distribution at different radial positions for different sample thicknesses: row1) height=10mm, row 2) height=50mm, & row 3) height=100mm .....	106
Figure 72: Radius-wise radial stress distribution at different axial positions for different sample thicknesses: row1) height=10mm, row 2) height=50mm, & row 3) height=100mm .....	107
Figure 73: Radial stress evolution at different axial positions for different sample thicknesses: row1) height=10mm, row 2) height=50mm, & row 3) height=100mm .....	108
Figure 74: Height-wise shear stress distribution at different radial positions for different sample thicknesses: row1) height=10mm, row 2) height=50mm, & row 3) height=100mm .....	110
Figure 75: Radius-wise shear stress distribution at different axial positions for different sample thicknesses: row1) height=10mm, row 2) height=50mm, & row 3) height=100mm .....	111
Figure 76: Shear stress evolution at different axial positions for different sample thicknesses: row1) height=10mm, row 2) height=50mm, & row 3) height=100mm .....	112
Figure 77: Current density evolution at different axial positions for different sample thicknesses: row1) height=10mm, row 2) height=50mm, & row 3) height=100mm .....	114
Figure 78: Height-wise temperature distribution at different radial positions for different sample thicknesses: row1) height=10mm, row 2) height=50mm, & row 3) height=100mm .....	116
Figure 79: Radius-wise temperature distribution at different axial positions for different sample thicknesses: row1) height=10mm, row 2) height=50mm, & row 3) height=100mm .....	117
Figure 80: Temperature evolution at different axial positions for different sample thicknesses: row1) height=10mm, row 2) height=50mm, & row 3) height=100mm .....	118

Figure 81: Height-wise von-Mises stress distribution at different radial positions for different sample thicknesses: row1) height=10mm, row 2) height=50mm, & row 3) height=100mm .....	120
Figure 82: Radius-wise von-Mises stress distribution at different axial positions for different sample thicknesses: row1) height=10mm, row 2) height=50mm, & row 3) height=100mm .....	121
Figure 83: Von-Mises stress evolution at different axial positions for different sample thicknesses: row1) height=10mm, row 2) height=50mm, & row 3) height=100mm .....	122
Figure 84: Height-wise axial stress distribution at different radial positions for different sample thicknesses: row1) height=10mm, row 2) height=50mm, & row 3) height=100mm .....	124
Figure 85: Radius-wise axial stress distribution at different axial positions for different sample thicknesses: row1) height=10mm, row 2) height=50mm, & row 3) height=100mm .....	125
Figure 86: Axial stress evolution at different axial positions for different sample thicknesses: row1) height=10mm, row 2) height=50mm, & row 3) height=100mm .....	126
Figure 87: Height-wise radial stress distribution at different radial positions for different sample thicknesses: row1) height=10mm, row 2) height=50mm, & row 3) height=100mm .....	128
Figure 88: Radius-wise radial stress distribution at different axial positions for different sample thicknesses: row1) height=10mm, row 2) height=50mm, & row 3) height=100mm .....	129
Figure 89: Radial stress evolution at different axial positions for different sample thicknesses: row1) height=10mm, row 2) height=50mm, & row 3) height=100mm .....	130
Figure 90: Height-wise shear stress distribution at different radial positions for different sample thicknesses: row1) height=10mm, row 2) height=50mm, & row 3) height=100mm .....	132
Figure 91: Radius-wise shear stress distribution at different axial positions for different sample thicknesses: row1) height=10mm, row 2) height=50mm, & row 3) height=100mm .....	133
Figure 92: Shear stress evolution at different axial positions for different sample thicknesses: row1) height=10mm, row 2) height=50mm, & row 3) height=100mm .....	134

## LIST OF TABLES

Table 1: Summary of the literature review. ....	24
Table 2: Dimensions of the used geometry.....	50
Table 3: Thermo-physical properties of the materials used in the study .....	54

## NOMENCLATURE

$A_{cr}$	Material constant
$C_p$	Specific heat
$P_L$	Effective sintering stress
$Q$	Volumetric heat sources
$\dot{\epsilon}$	Shrinkage rate
$k_T$	Thermal conductivity
$\vec{q}$	Heat flux vector
$r_o$	Average particle radius
$\dot{\gamma}$	Shape change rate
$\delta_{ij}$	Kronekar's delta
$\dot{\epsilon}$	Steady-state creep rate
$\epsilon_{ij}$	Strain rate components
$\sigma_{ij}$	Externally applied stress
$B$	Burger's vector
$D$	Diffusivity
$E$	Electric field intensity
$J$	Electric current density
$k$	Boltzman's constant
$n$	Material constant
$h$	Heat transfer coefficient
$T$	Absolute temperature
$t$	Time
$V$	Electric potential
$V_o$	Applied voltage
$W$	Equivalent strain rate
$\alpha$	Surface energy
$\lambda$	Electrical conductivity
$\mu$	Shear modulus
$\rho$	Mass density
$\sigma(W)$	Effective stress
$\varphi$	Normalized shear viscosity modulus
$\psi$	Normalized bulk viscosity modulus
$\epsilon_r$	Relative permittivity
$\epsilon_o$	Permittivity of free space
$\nabla T$	Temperature gradient



MULTIPHYSICS MODELING OF THE SPARK PLASMA SINTERING -SPS- PROCESS	العنوان:
Luqman, Muhammad	المؤلف الرئيسي:
Nouari, Saheb(super.)	مؤلفين آخرين:
2014	التاريخ الميلادي:
الظهران	موقع:
1 - 134	الصفحات:
651624	رقم MD:
رسائل جامعية	نوع المحتوى:
English	اللغة:
رسالة ماجستير	الدرجة العلمية:
جامعة الملك فهد للبترول والمعادن	الجامعة:
عمادة الدراسات العليا	الكلية:
السعودية	الدولة:
Dissertations	قواعد المعلومات:
النمذجة، الهندسة الميكانيكية	مواضيع:
<a href="https://search.mandumah.com/Record/651624">https://search.mandumah.com/Record/651624</a>	رابط:



**MULTIPHYSICS MODELING OF THE SPARK**

**PLASMA SINTERING (SPS) PROCESS**

BY

**MUHAMMAD LUQMAN**

A Thesis Presented to the  
DEANSHIP OF GRADUATE STUDIES

**KING FAHD UNIVERSITY OF PETROLEUM & MINERALS**

DHAHRAN, SAUDI ARABIA

In Partial Fulfillment of the  
Requirements for the Degree of

**MASTER OF SCIENCE**

In

**MECHANICAL ENGINEERING**

MARCH 2014

KING FAHD UNIVERSITY OF PETROLEUM & MINERALS

DHAHRAN- 31261, SAUDI ARABIA

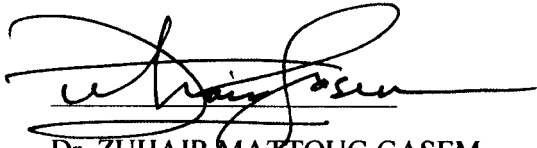
DEANSHIP OF GRADUATE STUDIES

This thesis, written by **Mr. MUHAMMAD LUQMAN** under the direction of his thesis advisor and approved by his thesis committee, has been presented and accepted by the Dean of Graduate Studies, in partial fulfillment of the requirements for the degree of **MASTER OF SCIENCE IN MECHANICAL ENGINEERING.**



Dr. NOUARI SAHEB

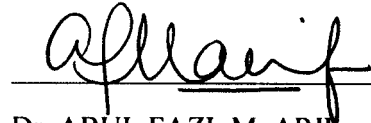
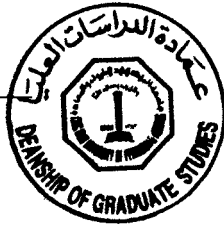
(Advisor)



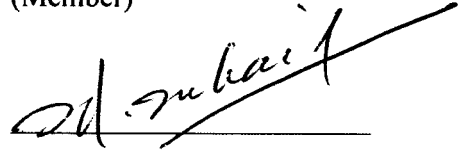
Dr. ZUHAIR MATTOUG GASEM  
Department Chairman



Dr. SALAM A. ZUMMO  
Dean of Graduate Studies



Dr. ABUL FAZL M. ARIF  
(Member)



Dr. SYED SOHAIL AKHTAR  
(Member)

30/2/14

Date

© Muhammad Luqman

2014

*Dedicated to my beloved parents, sisters and brothers.*

## ACKNOWLEDGMENTS

All praise belongs to ALLAH, the Almighty, who created the universe and sustains it; and Durud and Salam be on the last of all the prophets (صلي الله عليه وسلم) who made the truth prevail over falsehood and provided humanity with guidance for all times.

I sincerely acknowledge the support and facilities provided by King Fahd University of Petroleum & Minerals (KFUPM), Dhahran, Saudi Arabia. In addition to this, I would like to pay my deepest gratitude to the Center of Excellence in NanoTechnology (CENT), in the Research Institute, along with its team, for the exceptional knowledge and expertise that I gained during my tenure.

I would like to express my deepest appreciation to my thesis advisor Dr. Nouari Saheb for his moral support and sincere advices; he continually and persuasively conveyed a spirit of adventure in regard to research. In addition to my advisor, I'm also grateful to my thesis committee members, Prof. Abul Fazl Muhammad Arif and Dr. Syed Sohail Akhtar for their valuable contributions, guidance, support and encouragement throughout my research. Furthermore, special thanks are due to Dr. Abbas Saeed Hakeem for his guidance and support in the experimental work.

I would also like to express my deepest gratitude to the faculty members of the Mechanical Engineering Department at KFUPM. Moreover, I'm deeply indebted to Mr. Abdullatif Hashmi and Mr. Sadaqat for their support and cooperation in the experimental work.

I would also like to express my sincere appreciation to my colleagues in the Mechanical Engineering department, especially Mr. Abdul Azeem & Mr. Najm-ul-Qadir for helping me in different aspects of the thesis' work. Additionally, I'd like to acknowledge my friends Muhammad Usman, Raja Muhammad Awais, Waleed Umar, Waseem Razzaq, Muhammad Nasir, Muhammad Umer Khan, Saad Muhammad Saad Khan, Hassaan Ahmed, Uneb Gazder and Muhammad Qamar. Without their help, it would have been impossible for me to finish my M.S. study.

Last, but not the least, I would like to thank my parents for their endless love and support; who, although far away from me, were always close to my thoughts and heart. I would also like to thank my sisters and brothers for their moral support and encouragement.

# TABLE OF CONTENTS

ACKNOWLEDGMENTS .....	iv
TABLE OF CONTENTS.....	v
LIST OF FIGURES .....	viii
LIST OF TABLES .....	xiv
NOMENCLATURE .....	xv
ABSTRACT.....	xvi
ملخص الرسالة.....	xviii
CHAPTER 1 .....	1
INTRODUCTION .....	1
1.1    SPARK PLASMA SINTERING (SPS) .....	2
1.1.1    Instrumentation.....	2
1.1.2    Sintering procedure.....	2
1.1.3    Electrical transport in SPS process .....	3
1.1.4    Heating mechanism in SPS process.....	4
1.1.5    Loading mechanism in SPS process .....	6
1.1.6    Advantages of SPS .....	6
1.1.7    Difficulties in SPS process .....	8
1.1.8    Differences between conventional and non-conventional sintering mechanisms .....	8
1.2    MOTIVATION .....	9
1.3    OBJECTIVES .....	10
CHAPTER 2 .....	11
LITERATURE REVIEW .....	11
2.1    THERMAL-ELECTRICAL MODELING .....	12

2.2	STRUCTURAL MODELING .....	22
CHAPTER 3 .....		27
EXPERIMENTAL STUDY.....		27
3.1	INTRODUCTION.....	27
3.2	EXPERIMENTAL TECHNIQUES .....	27
3.2.1	Particles' Size Analysis .....	27
3.2.2	X-Ray Diffraction.....	28
3.2.3	Micro-hardness Testing .....	30
3.2.4	Scanning Electron Microscope .....	31
3.3	RAW MATERIALS.....	32
3.3.1	Aluminum powder.....	32
3.3.2	Alumina powder .....	34
3.4	SPARK PLASMA SINTERING (SPS) .....	36
3.5	RESULTS.....	38
3.5.1	Sample Preparation.....	38
3.5.2	Hardness Test .....	38
3.5.3	Microstructure .....	41
CHAPTER 4 .....		44
ELECTRICAL-THERMAL MODEL .....		44
4.1	INTRODUCTION.....	44
4.2	THE MODEL.....	45
4.2.1	Mathematical Model.....	45
4.2.2	Model in COMSOL Multiphysics .....	49
4.3	RESULTS & DISCUSSION.....	55
4.3.1	General Observations about the whole system .....	55



4.3.2	Validation of the developed model.....	61
4.3.3	CASE-I .....	63
4.3.4	CASE-II.....	75
CHAPTER 5 .....		82
STRUCTURAL MODEL .....		82
5.1	INTRODUCTION.....	82
5.2	THE MODEL.....	82
5.2.1	Mathematical model .....	82
5.2.2	Model in COMSOL Multiphysics .....	85
5.3	RESULTS AND DISCUSSIONS .....	86
5.3.1	Validation of the developed model.....	86
5.3.2	CASE-I .....	89
5.3.3	CASE-II.....	113
CHAPTER 6 .....		135
CONCLUSIONS & RECOMMENDATIONS.....		135
6.1	CONCLUSIONS.....	136
6.2	RECOMMENDATIONS .....	137
REFERENCES .....		139
VITAE.....		143

## LIST OF FIGURES

Figure 1: Schematic of SPS Process [1] .....	2
Figure 2: Different pulse patterns in pulsed DC power supply [2].....	4
Figure 3: SPS Sintering mechanism; Plasma heating (left), & Joule heating (right) [3]....	5
Figure 4: Densification mechanism in SPS [3].....	6
Figure 5: Comparison of sintering time and temp. Of SPS and conventional sintering [6].....	7
Figure 6: Integration domain and boundary conditions of the model proposed by Raichenko and Chernikova [9]. .....	12
Figure 7: Integration domain and boundary conditions of the model proposed by Yoneya and Ikeshoji [10].....	14
Figure 8: Integration domain of the model proposed by Matsugi et al [13].....	16
Figure 9: Simulation results for die diameter and die height at a sample center temperature of 1,800°C. Solid points represent simulations including radiation, and hollow points are simulation results with die wall radiation blocked. [5] .....	19
Figure 10: Complex shaped part sintered by Spark Plasma Sintering [21] .....	21
Figure 11: Schematic of X-Rays diffraction.....	29
Figure 12: Schematic of micro-hardness test.....	31
Figure 13: Electron-sample interactions. ....	32
Figure 14: Particle size distribution of as-received aluminum powder. ....	33
Figure 15: Microstructure of as-received aluminum powder. ....	33
Figure 16: XRD spectrum of as received Aluminum powder .....	34
Figure 17 : Particle size distribution of as-received alumina powder.....	35
Figure 18: Microstructure of as-received alumina powder.....	35
Figure 19: XRD spectrum of as received Alumina powder.....	36
Figure 20: Die-punch system during sintering of alumina samples .....	37
Figure 21: Positions of the hardness test.....	39

Figure 22: Hardness (HV) along the radius at different heights in aluminum sample .....	40
Figure 23: Hardness (HV) along the height at different radial positions in aluminum sample .....	40
Figure 24: Hardness (HV) along the radius at different heights in alumina sample.....	41
Figure 25: Hardness (HV) along the height at different radial positions in alumina sample .....	41
Figure 26: SEM micrographs of the aluminum sample at 1000x magnification at different locations: A1, A3, A5, C1, C3, C5, E1, E3, & E5 .....	42
Figure 27: SEM micrographs of the aluminum sample at 500x magnification at different locations: A1, A3, A5, C1, C3, C5, E1, E3, & E5 .....	43
Figure 28: Schematic of the die-punch-specimen system in SPS process.....	49
Figure 29: Model Geometry in COMSOL Multiphysics environment.....	50
Figure 30: Domains and boundaries in the model. ....	51
Figure 31: The Applied voltage .....	52
Figure 32: Meshes used in the model: Left) mapped, & Right) triangular.....	53
Figure 33: Surface Current density contour plot for sample height=50 mm, at 650s.....	56
Figure 34: Surface Current density contour plot for sample height=100 mm, at 650s.....	56
Figure 35: Surface Temperature contour plot for sample height=50mm, at t=650s.....	57
Figure 36: Surface Temperature contour plot for sample height=100mm, at t=650s.....	58
Figure 37: Graph showing the temperature evolution in punches .....	58
Figure 38: Graph showing the temperature evolution in the sample .....	59
Figure 39: Graph showing average temperature evolution in sample for different sample heights.....	59
Figure 40: Divisions in the sample. ....	60
Figure 41: Current density distribution along the radius: Left) this study, & Right) F. Mechighel et. Al. [32].....	61
Figure 42: Temperature distribution along the radius: Left) this study, & Right) F. Mechighel et. Al [32].....	62

Figure 43: Current density plots at: (left) $t=350s$ , & (right) $t=600s$ .....	65
Figure 44: (Left) Current density in the system, & (right) corresponding Total heat source in the system at $t=1200s$ .....	65
Figure 45: Current density distribution along radius at different axial positions for different sample thicknesses: row1) height=10mm, row 2) height=50mm, & row 3) height=100mm .....	66
Figure 46: Current density distribution along height at different radial positions for different sample thicknesses: row1) height=10mm, row 2) height=50mm, & row 3) height=100mm .....	67
Figure 47: Current density evolution at different locations for different sample thicknesses: row1) height=10mm, row 2) height=50mm, & row 3) height=100mm .....	68
Figure 48: Temperature distribution in the system at different timings at: (left) $t=600s$ , & (right) $t=1200s$ . .....	70
Figure 49: Temperature distribution along radius at different axial positions for different sample thicknesses: row1) height=10mm, row 2) height=50mm, & row 3) height=100mm .....	71
Figure 50: Temperature distribution along height at different radial positions for different sample thicknesses: row1) height=10mm, row 2) height=50mm, & row 3) height=100mm .....	72
Figure 51: Temperature evolution at different locations for different sample thicknesses: row1) height=10mm, row 2) height=50mm, & row 3) height=100mm .....	73
Figure 52: Current density evolution at different locations for different sample thicknesses: row1) height=10mm, row 2) height=50mm, & row 3) height=100mm .....	77
Figure 53: Temperature distribution along radius at different axial positions for different sample thicknesses: row1) height=10mm, row 2) height=50mm, & row 3) height=100mm .....	78
Figure 54: Temperature distribution along height at different radial positions for different sample thicknesses: row1) height=10mm, row 2) height=50mm, & row 3) height=100mm .....	79
Figure 55: Temperature evolution at different locations for different sample thicknesses: row1) height=10mm, row 2) height=50mm, & row 3) height=100mm .....	80

Figure 56: The Applied pressure.....	86
Figure 57: Axial stress distribution along the radius in the sample: Left) this study, & Right) F. Mechighel et. Al [32] .....	87
Figure 58: Radial stress distribution along the radius in the sample: Left) this study, & Right) F. Mechighel et. Al [32] .....	88
Figure 59: Current density along height at different radial positions for different sample thicknesses: row1) height=10mm, row 2) height=50mm, & row 3) height=100mm .....	90
Figure 60: Current density along radius at different axial positions for different sample thicknesses: row1) height=10mm, row 2) height=50mm, & row 3) height=100mm .....	91
Figure 61: Current density evolution at different axial positions for different sample thicknesses: row1) height=10mm, row 2) height=50mm, & row 3) height=100mm .....	92
Figure 62: Height-wise temperature distribution at different radial positions for different sample thicknesses: row1) height=10mm, row 2) height=50mm, & row 3) height=100mm .....	94
Figure 63: Radius-wise temperature distribution at different radial positions for different sample thicknesses: row1) height=10mm, row 2) height=50mm, & row 3) height=100mm .....	95
Figure 64: Temperature evolution at different axial positions for different sample thicknesses: row1) height=10mm, row 2) height=50mm, & row 3) height=100mm .....	96
Figure 65: Height-wise von-Mises stress distribution at different radial positions for different sample thicknesses: row1) height=10mm, row 2) height=50mm, & row 3) height=100mm .....	98
Figure 66: Radius-wise von-Mises stress distribution at different axial positions for different sample thicknesses: row1) height=10mm, row 2) height=50mm, & row 3) height=100mm .....	99
Figure 67: Von-Mises stress evolution at different axial positions for different sample thicknesses: row1) height=10mm, row 2) height=50mm, & row 3) height=100mm .....	100
Figure 68: Height-wise axial stress distribution at different radial positions for different sample thicknesses: row1) height=10mm, row 2) height=50mm, & row 3) height=100mm .....	102

Figure 69: Radius-wise axial stress distribution at different axial positions for different sample thicknesses: row1) height=10mm, row 2) height=50mm, & row 3) height=100mm .....	103
Figure 70: Axial stress evolution at different axial positions for different sample thicknesses: row1) height=10mm, row 2) height=50mm, & row 3) height=100mm .....	104
Figure 71: Height-wise radial stress distribution at different radial positions for different sample thicknesses: row1) height=10mm, row 2) height=50mm, & row 3) height=100mm .....	106
Figure 72: Radius-wise radial stress distribution at different axial positions for different sample thicknesses: row1) height=10mm, row 2) height=50mm, & row 3) height=100mm .....	107
Figure 73: Radial stress evolution at different axial positions for different sample thicknesses: row1) height=10mm, row 2) height=50mm, & row 3) height=100mm .....	108
Figure 74: Height-wise shear stress distribution at different radial positions for different sample thicknesses: row1) height=10mm, row 2) height=50mm, & row 3) height=100mm .....	110
Figure 75: Radius-wise shear stress distribution at different axial positions for different sample thicknesses: row1) height=10mm, row 2) height=50mm, & row 3) height=100mm .....	111
Figure 76: Shear stress evolution at different axial positions for different sample thicknesses: row1) height=10mm, row 2) height=50mm, & row 3) height=100mm .....	112
Figure 77: Current density evolution at different axial positions for different sample thicknesses: row1) height=10mm, row 2) height=50mm, & row 3) height=100mm .....	114
Figure 78: Height-wise temperature distribution at different radial positions for different sample thicknesses: row1) height=10mm, row 2) height=50mm, & row 3) height=100mm .....	116
Figure 79: Radius-wise temperature distribution at different axial positions for different sample thicknesses: row1) height=10mm, row 2) height=50mm, & row 3) height=100mm .....	117
Figure 80: Temperature evolution at different axial positions for different sample thicknesses: row1) height=10mm, row 2) height=50mm, & row 3) height=100mm .....	118

Figure 81: Height-wise von-Mises stress distribution at different radial positions for different sample thicknesses: row1) height=10mm, row 2) height=50mm, & row 3) height=100mm .....	120
Figure 82: Radius-wise von-Mises stress distribution at different axial positions for different sample thicknesses: row1) height=10mm, row 2) height=50mm, & row 3) height=100mm .....	121
Figure 83: Von-Mises stress evolution at different axial positions for different sample thicknesses: row1) height=10mm, row 2) height=50mm, & row 3) height=100mm .....	122
Figure 84: Height-wise axial stress distribution at different radial positions for different sample thicknesses: row1) height=10mm, row 2) height=50mm, & row 3) height=100mm .....	124
Figure 85: Radius-wise axial stress distribution at different axial positions for different sample thicknesses: row1) height=10mm, row 2) height=50mm, & row 3) height=100mm .....	125
Figure 86: Axial stress evolution at different axial positions for different sample thicknesses: row1) height=10mm, row 2) height=50mm, & row 3) height=100mm .....	126
Figure 87: Height-wise radial stress distribution at different radial positions for different sample thicknesses: row1) height=10mm, row 2) height=50mm, & row 3) height=100mm .....	128
Figure 88: Radius-wise radial stress distribution at different axial positions for different sample thicknesses: row1) height=10mm, row 2) height=50mm, & row 3) height=100mm .....	129
Figure 89: Radial stress evolution at different axial positions for different sample thicknesses: row1) height=10mm, row 2) height=50mm, & row 3) height=100mm .....	130
Figure 90: Height-wise shear stress distribution at different radial positions for different sample thicknesses: row1) height=10mm, row 2) height=50mm, & row 3) height=100mm .....	132
Figure 91: Radius-wise shear stress distribution at different axial positions for different sample thicknesses: row1) height=10mm, row 2) height=50mm, & row 3) height=100mm .....	133
Figure 92: Shear stress evolution at different axial positions for different sample thicknesses: row1) height=10mm, row 2) height=50mm, & row 3) height=100mm .....	134

## LIST OF TABLES

Table 1: Summary of the literature review. ....	24
Table 2: Dimensions of the used geometry.....	50
Table 3: Thermo-physical properties of the materials used in the study .....	54



## NOMENCLATURE

$A_{cr}$	Material constant
$C_p$	Specific heat
$P_L$	Effective sintering stress
$Q$	Volumetric heat sources
$\dot{\epsilon}$	Shrinkage rate
$k_T$	Thermal conductivity
$\vec{q}$	Heat flux vector
$r_o$	Average particle radius
$\dot{\gamma}$	Shape change rate
$\delta_{ij}$	Kronekar's delta
$\dot{\epsilon}$	Steady-state creep rate
$\epsilon_{ij}$	Strain rate components
$\sigma_{ij}$	Externally applied stress
$B$	Burger's vector
$D$	Diffusivity
$E$	Electric field intensity
$J$	Electric current density
$k$	Boltzman's constant
$n$	Material constant
$h$	Heat transfer coefficient
$T$	Absolute temperature
$t$	Time
$V$	Electric potential
$V_o$	Applied voltage
$W$	Equivalent strain rate
$\alpha$	Surface energy
$\lambda$	Electrical conductivity
$\mu$	Shear modulus
$\rho$	Mass density
$\sigma(W)$	Effective stress
$\varphi$	Normalized shear viscosity modulus
$\psi$	Normalized bulk viscosity modulus
$\epsilon_r$	Relative permittivity
$\epsilon_o$	Permittivity of free space
$\nabla T$	Temperature gradient

## ABSTRACT

Full Name : Muhammad Luqman  
Thesis Title : Multi-Physics Modeling Of The Spark Plasma Sintering (SPS) Process  
Major Field : Mechanical Engineering  
Date of Degree : March, 2014

Spark plasma sintering (SPS) is defined as a processing technique, which sinters materials using electric current in conjunction with uniaxial pressure. It offers several advantages over conventional techniques like achievement of near-theoretical density and nanocrystalline morphology in extremely shorter sintering durations, avoidance of abnormal grain growth, and clean sample surfaces due to interaction with gaseous plasma. However, the major drawbacks of SPS which are not observed in conventional sintering techniques include difficulty in sintering complex-shaped or large-sized samples, relatively large degree of inhomogeneity in mechanical properties, and charge accumulation especially in insulating powders. Hence in order to achieve the best processing results, it is obligatory to grasp a firm understanding of the kinetics of SPS process. Since experimental methods do not facilitate the in-situ measurement of sintering temperature, pressure, and relative density, one has to rely on computational techniques in order to get a better understanding of the process kinetics. These computational techniques are utilized in predicting the structure-property relationship of the material being sintered, and optimization of the process parameters in order to achieve the best mechanical properties without presence of inhomogeneity. The main

objective of the computational work done in this study is to develop a coupled electrical–thermal–mechanical Finite Element Model of the SPS process. This model has been used to study two different classes of materials – aluminum (an electrical conductor), and alumina (an electrical insulator), where a range of aspect ratios has been considered for each disk-shaped sample. In order to validate the results obtained via computational analysis, a small-scale experimental study is also conducted to determine the relationship between SPS process-parameters and the mechanical properties of sintered sample. Comparison of the results obtained from the computational model with those achieved from the experimental study, indicate that almost all the process parameters as well as mechanical properties are characterized by inhomogeneity within the sintered samples.

## ملخص الرسالة

الاسم الكامل : محمد لقمان

عنوان الرسالة : متعدد الفيزياء نمذجة البلازما التكلس سبارك (SPS). عملية

التخصص : الهندسة الميكانيكية

تاريخ الدرجة العلمية : مارس 2014

يتم تعريف تكلس شرارة البلازما (SPS) كأسلوب معالجة، والتي تكلس المواد باستخدام التيار الكهربائي بالتزامن مع الضغط أحادي المحور. أنها توفر العديد من المزايا أكثر من التقنيات التقليدية مثل تحقيق الكثافة شبه النظرية، وتشكل البلورات النانوية في فترات تكلس قصيرة للغاية، متجنبة نمو الحبوب الغير طبيعية، وسطوح العينات النظيفة بسبب التفاعل مع غازات البلازما. ومع ذلك، فإن العوائق الرئيسية لتكلس شرارة البلازما التي لم تلاحظ في تقنيات التكلس التقليدية تشمل صعوبة في تكلس العينات ذو الأشكال المعقدة أو كبيرة الحجم، نسبيًا درجة عالية من عدم التجانس في الخصائص الميكانيكية، وتراكم الشحنات خاصة في عزل المساحيق. وبالتالي من أجل تحقيق أفضل النتائج المعالجة، يجب الإمساك بالفهم الراسخ لحركية تكلس شرارة البلازما. و بما أن الطرق التجريبية لا تسهل قياس درجة الحرارة و الضغط و الكثافة النسبية للتكلس أثناء اجراء التجربة، على المرء الاعتماد على التقنيات الحاسوبية من أجل الحصول على فهم أفضل للعملية الحركية. وتستخدم هذه التقنيات الحاسوبية في التنبؤ بعلاقة مميزات البنية للمواد الجاري تكلسها ، والاستفادة المثلى من معايير العملية من أجل تحقيق أفضل الخواص الميكانيكية في غياب عدم التجانس. الهدف الرئيسي من هذا العمل الحسابي في هذه الدراسة هو تطوير عناصر محدودة مقترنة كهربائيا وحراريا وميكانيكيا باستخدام عملية تكلس شرارة البلازما. وقد استخدم هذا النموذج لدراسة فئتين مختلفتين من المواد - الألومنيوم (موصل كهربائي) والألومينا (عازل كهربائي). حيث تم اعتبار مجموعة ذو نسب مختلفة من نسب العرض للطول لكل عينة على شكل القرص. من أجل التحقق من صحة النتائج التي تم الحصول عليها عن طريق التحليل الحسابي، أجرت دراسة تجريبية على نطاق ضيق لتحديد العلاقة بين عملية المتغيرات لتكلس شرارة البلازما والخواص الميكانيكية للعينة المتكلسة.

المقارنة بين النتائج تم الحصول عليها من النموذج الحسابي مع تلك التي تحققت من دراسة تجريبية، تشير إلى أن جميع المتغيرات وكذلك الخواص الميكانيكية تتميز بعدم التجانس في حدود العينات المتكلسة.

# CHAPTER 1

## INTRODUCTION

Spark Plasma Sintering (SPS) is a sintering technique which incorporates both uniaxial pressure and application of electric current to accelerate the sintering process. This technique offers various advantages over conventional sintering methods, e.g., faster heating rate, shorter sintering time, higher rate of powder densification, achievement of grain size in the nanocrystalline regime and near-theoretical density, cleanliness of near-surface particles by plasma ions, and avoidance of abnormal grain growth. The foremost advantage of SPS is achievement of near-theoretical density during sintering of ceramic powders characterized by high melting point and lower self-diffusion rate due to the existence of covalent bonding. However, the major disadvantage of this technique is the existence of thermal and mechanical gradient along the sample cross-section due to high heating rates, especially in case of ceramic and polymeric powders which are characterized by low values of electrical and thermal conductivity.

The fundamental mechanism of SPS is not well known. However, it is hypothesized that the interaction of electric current with the particles results in micro-sparks, which eventually leads to the removal of surface impurities and accelerates the surface and grain-boundary diffusion kinetics. A number of mathematical models, simulating the effect of SPS process parameters on the density evolution of the sample, have been proposed and implemented in Finite Element-based softwares including ABAQUS, ANSYS, CFD and COMSOL Multiphysics. In the present work, COMSOL Multiphysics has been used to simulate the electrical, thermal and mechanical

gradients along the cross-section of aluminum and alumina powders, sintered using the SPS process under a variety of heating rates.

## 1.1 SPARK PLASMA SINTERING (SPS)

### 1.1.1 Instrumentation

The SPS machine is composed of a uniaxial press, vacuum chamber (or controlled atmosphere), two punch electrodes, a die, a DC pulse generator, a controller/computing unit, and sensors to monitor the temperature, pressure and punch position. A generalized schematic highlighting the primary SPS instrumentation is shown in Figure 1.

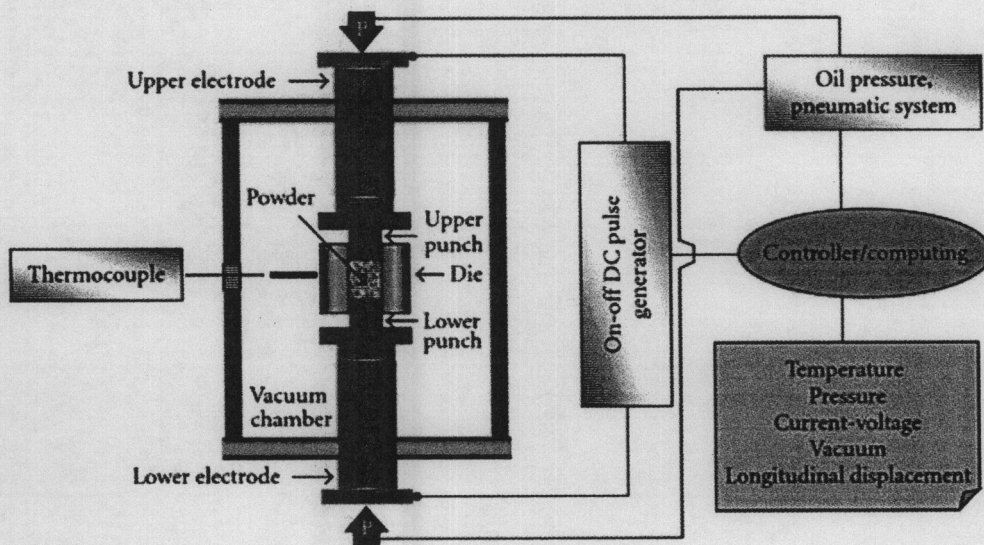


Figure 1: Schematic of SPS Process [1]

### 1.1.2 Sintering procedure

In SPS process, an electrical current is applied concurrently with a uniaxial mechanical pressure to sinter/consolidate powders for specific applications with preferred density and configuration. The applied mechanical load and electrical current can be kept

constant during the course of the sintering cycle, or can be varied during the subsequent densification stages. The powder to be sintered is placed in a die and then heated via application of electrical current. For electrically conducting powders, the following types of dies can be used:

- Electrically conducting die,
- Electrically insulating die (as the powder itself guarantees the electrical circuit closure), or
- A conducting die having non-conducting coating on the interior surface.

For insulating powders, the die material must be conducting in order to fulfill the requirement of a closed electrical circuit to initiate the sintering process. For the same reason, all the other components of the system, i.e., electrodes, blocks, spacers, and plungers etc. need to be made of an electrically conducting material, e.g. stainless steel, copper, graphite, etc.

### 1.1.3 Electrical transport in SPS process

The flow of electrical charge through the die-specimen system in SPS process relies primarily on the power supply characteristics, and thus can be characterized by different intensities and waveforms. However, irrespective of the waveform of the electrical current, the root mean squared value of the instantaneous intensity of the applied current can be expressed as:

$$I_{\text{RMS}} = \sqrt{\frac{1}{\tau} \int_t^{t+\tau} I^2(t) dt}$$

Where; “ $I$ ” denotes the instantaneous current, and “ $t$ ” represents the sampling time. Generally, in case of DC power supply, the applied voltage can be only a few volts (e.g. 0-10 V) and the current can be a several thousand Amperes (e.g. 1000-10,000 A). In case of pulsed DC power supply, the ON and OFF timings are usually in the range of a few milliseconds. The different types of pulse patterns that can be observed in the DC power supply are shown in Figure 2.

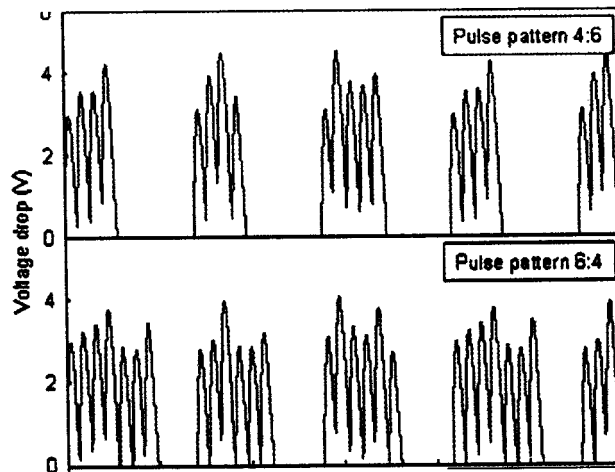


Figure 2: Different pulse patterns in pulsed DC power supply [2]

#### 1.1.4 Heating mechanism in SPS process

The foremost difference between heating mechanism in SPS process and other sintering techniques is that internal heat generation occurs exclusively due to the Joule effect of the DC current. The total heat generation in SPS process is a combination of two components:

- a. Heat generation in the die and punches, and
- b. Heat generation in the sample

In case of a conducting powder sample, the sample is heated both by the heat generated in the sample itself as well as by conduction of heat from electrodes and the



die. However, insulating powders are heated only by the conduction of the heat generated in the dies and the electrodes.

Although, the true mechanism of heat generation in SPS is still unclear, the heat generated in SPS is hypothetically attributed to the micro-spark discharge (plasma heating) in the gaps between neighboring powder particles, resulting in neck formation, which establishes a path for the conduction of electrical current through the particles. It is then followed by Joule heating, originating from the resistance of the material to the electrical current flowing through it, resulting in the coarsening of the grains (see Figure 3). As this heat generation has a localized character and almost uniform distribution, it allows rapid temperature rise and drop, which prohibits coarsening (growth) of the material grains.

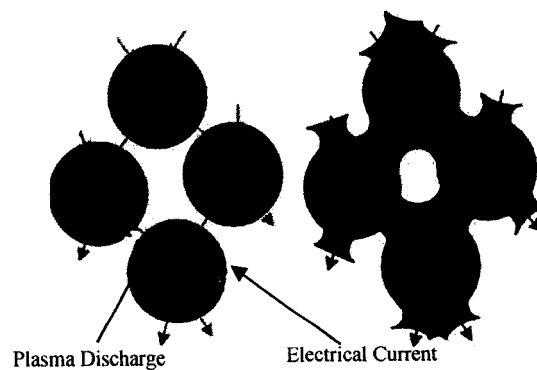


Figure 3: SPS Sintering mechanism; Plasma heating (left), & Joule heating (right) [3]

It is worth mentioning here that the only heat generation mechanism in the SPS process which is supported by experimental validation is the Joule effect. All other phenomena that are associated with the current flow – plasma formation, generation of sparks, high local temperature at the contact surfaces of the particles, etc. – may take

MULTIPHYSICS MODELING OF THE SPARK PLASMA SINTERING -SPS- PROCESS	العنوان:
Luqman, Muhammad	المؤلف الرئيسي:
Nouari, Saheb(super.)	مؤلفين آخرين:
2014	التاريخ الميلادي:
الظهران	موقع:
1 - 134	الصفحات:
651624	رقم MD:
رسائل جامعية	نوع المحتوى:
English	اللغة:
رسالة ماجستير	الدرجة العلمية:
جامعة الملك فهد للبترول والمعادن	الجامعة:
عمادة الدراسات العليا	الكلية:
السعودية	الدولة:
Dissertations	قواعد المعلومات:
النمذجة، الهندسة الميكانيكية	مواضيع:
<a href="https://search.mandumah.com/Record/651624">https://search.mandumah.com/Record/651624</a>	رابط:



**MULTIPHYSICS MODELING OF THE SPARK**

**PLASMA SINTERING (SPS) PROCESS**

BY

**MUHAMMAD LUQMAN**

A Thesis Presented to the  
DEANSHIP OF GRADUATE STUDIES

**KING FAHD UNIVERSITY OF PETROLEUM & MINERALS**

DHAHRAN, SAUDI ARABIA

In Partial Fulfillment of the  
Requirements for the Degree of

**MASTER OF SCIENCE**

In

**MECHANICAL ENGINEERING**

MARCH 2014